Chemical Science

ROYAL SOCIETY OF CHEMISTRY

EDGE ARTICLE

View Article Online
View Journal | View Issue

Cite this: *Chem. Sci.*, 2024, **15**, 14352

All publication charges for this article have been paid for by the Royal Society of Chemistry

Received 25th April 2024
Accepted 1st August 2024

DOI: 10.1039/d4sc02736a

rsc.li/chemical-science

Fusion of two homoleptic truncated tetrahedra into a heteroleptic truncated octahedron†

Haifei Liu,‡[a] Chenxing Guo, ‡[b] Yujuan Huang,‡[a] Zilin Zhou,[a] Shijin Jian,[a] Zeyuan Zhang, [a] Yali Hou,[a] Chaoqun Mu*[c] and Mingming Zhang *[a]

The exploration of novel structures and structural transformation of supramolecular assemblies is of vital importance for their functions and applications. Herein, based on coordination-driven self-assembly, we prepare a neutral truncated tetrahedron and a heteroleptic truncated octahedron, whose structures are unambiguously confirmed by X-ray diffraction analysis. More importantly, the truncated tetrahedron is quantitatively transformed into the truncated octahedron through its fusion with another cationic truncated tetrahedron, as evidenced by fluorescence, mass and NMR spectroscopy. This study not only deepens our understanding of the process of supramolecular fusion but also opens up possibilities for the subsequent preparation of advanced supramolecular assemblies with complex structures and integrated functions.

Introduction

In natural systems, the structural transformation of biomolecules plays a crucial role in biological processes like enzymatic catalysis, signal transduction, allosteric regulation, *etc.*[1–3] Inspired by this, chemists have constructed a series of artificial systems to mimic biological transformations based on supramolecular self-assembly,[4–8] expecting to prepare advanced materials with sophisticated functions comparable to biomolecules. In this regard, fusion-based structural transformation has received much attention because it can integrate all the building blocks of precursors into the final constructs, forming assemblies with improved structural and functional complexity (Fig. 1).[9,10] However, such a process is highly challenging because elegant ligand design and tedious synthesis are generally required to prevent the formation of thermodynamic mixtures and meet the requirements of quantitative supramolecular transformation.

Owing to their moderate bond strength and fixed directionality, metal-coordination bonds have been widely used for the construction of two-dimensional metallacycles and three-dimensional metallacages,[11–23] which are further employed in molecular recognition, stabilization of active substances, catalysis, *etc.*[24–29] Moreover, these metal–organic assemblies are promising candidates for the construction of transformable supramolecular systems based on their dynamic and moderate stability. Although some progress has been made in this field,[9] fusion-based structural transformation, especially the fusion of two geometrically similar metallacages into a new structure, has

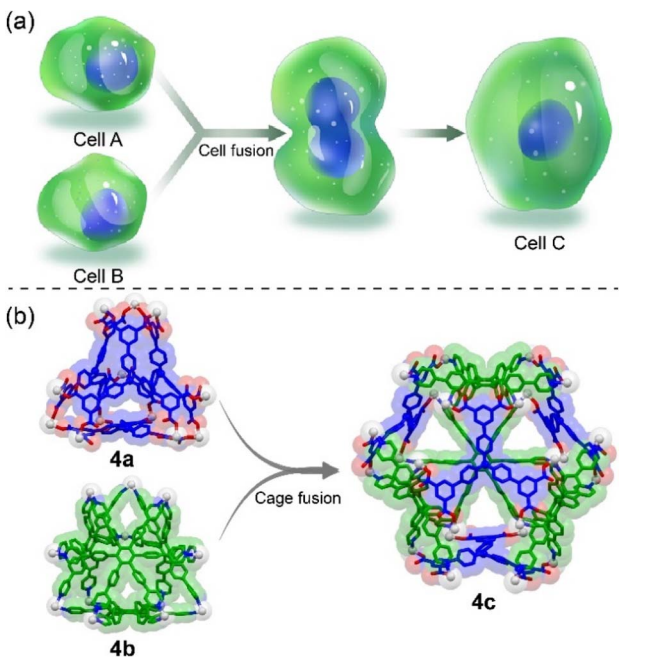

Fig. 1 Representations of (a) cell fusion and (b) cage fusion.

[a]*State Key Laboratory for Mechanical Behavior of Materials, Shaanxi International Research Center for Soft Matter, School of Materials Science and Engineering, Xi'an Jiaotong University, Xi'an 710049, P. R. China. E-mail: mingming.zhang@xjtu.edu.cn*
[b]*College of Chemistry and Environmental Engineering, Shenzhen University, Shenzhen 518055, P. R. China*
[c]*School of Chemistry and Chemical Engineering, Xi'an University of Architecture and Technology, Xi'an 710055, Shaanxi, P. R. China. E-mail: chaoqunmu@xauat.edu.cn*

† Electronic supplementary information (ESI) available. CCDC 2314346 (for **4a**) and 2314347 (for **4c**). For ESI and crystallographic data in CIF or other electronic format see DOI: https://doi.org/10.1039/d4sc02736a

‡ These authors contributed equally to this work.

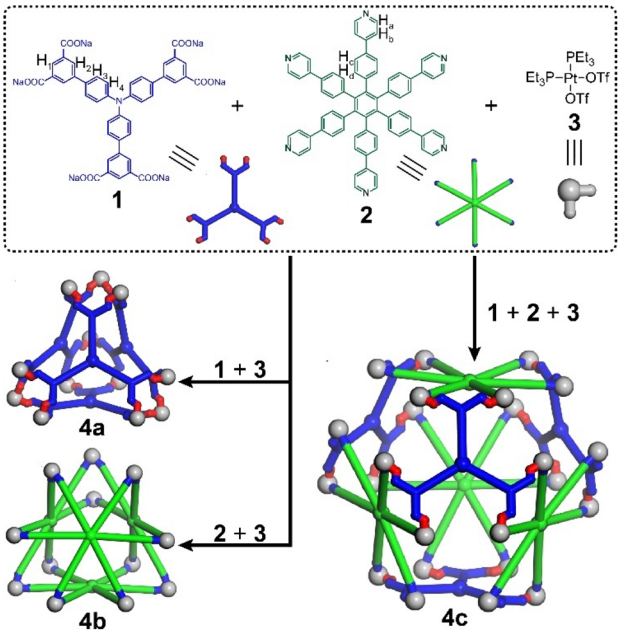

Fig. 2 Illustration of the self-assembly of metallacages 4a–4c.

been rarely reported, which is probably because it is difficult to design and prepare two complementary three-dimensional coordination assemblies for quantitative fusion. Such a study will not only deepen our understanding of the mechanism of biological and abiological fusion, but also offer new opportunities for the direct functional integration of different supramolecular assemblies. Therefore, the development of fusion-based supramolecular systems from three-dimensional self-assembled structures is highly demanding, yet challenging.

The Stang and Mukherjee groups pioneered the integrative self-assembly of pyridyl and carboxylic donors with metal acceptors *via* charge separation,[30–32] demonstrating its efficiency in preparing multicomponent metallacages. The heteroleptic self-assembly of platinum nodes with both multiple pyridyl and carboxylic ligands has also proved to be an efficient strategy for the construction of multicomponent metallacages in our group.[33–44] Moreover, the homoleptic self-assembly of platinum nodes with multiple pyridyl ligands also provides a series of two-component metallacages.[45,46] However, the preparation of metallacages *via* the self-assembly of platinum nodes with multiple carboxylic ligands has never been reported, although some metallacycles have been reported by this strategy,[30] which is due to the decreased solubility and difficult structural characterization of such neutral, three-dimensional supramolecular structures. Herein, based on metal-coordination-driven self-assembly, we prepare a neutral, truncated tetrahedral metallacage (**4a**) and a heteroleptic truncated octahedral metallacage (**4c**) (Fig. 2), whose structures are unambiguously confirmed by X-ray diffraction analysis. Interestingly, further assembly of **4a** with a previously reported cationic, truncated tetrahedron (**4b**)[45] leads to the quantitative formation of **4c**, due to the energy of the heteroleptic metallacage significantly being lower than that with two homoleptic metallacages,[30] representing a fusion-based supramolecular transformation from geometrically the same truncated tetrahedron-shaped metallacages. This study not only contributes to the construction of novel coordination structures but also explores their fusion-based structural transformation, which will promote the development of supramolecular assemblies with tunable structures and integrated functions.

Results and discussion

Metallacage **4a** or **4b** was prepared by the self-assembly of hexatopic carboxylic ligand **1** (L_1) or pyridyl ligand **2** (L_2) with *cis*-Pt$(PEt_3)_2(OTf)_2$ **3** (M), while metallacage **4c** was synthesized by the heteroleptic self-assembly of **1**, **2** and **3** (Fig. 2, see the ESI† for synthetic details). All the metallacages were characterized by 1D multinuclear ($^{31}P\{^1H\}$ and ^1H) NMR, 2D diffusion-ordered NMR spectroscopy (DOSY) and electrospray ionization time-of-flight mass spectroscopy (ESI-TOF-MS), as well as X-ray diffraction analysis. In the $^{31}P\{^1H\}$ NMR spectra (Fig. 3a and b), only one single peak was observed for metallacages **4a** ($M_{12}(L_1)_4$) at 2.52 ppm and **4b** ($M_{12}(L_2)_4$) at 0.47 ppm, agreeing well with the single phosphorus environment in their symmetric structures. For metallacage **4c** ($M_{24}(L_1)_4(L_2)_4$), two doublet peaks with equal intensities were found at 5.35 and 0.10 ppm (Fig. 3c), which is consistent with the different phosphorus environments after the coordination. In the ^1H NMR spectra, upfield chemical shifts were observed for protons H_1, H_2, H_3 and H_4 of **4a** compared with its carboxylic precursor **1** (Fig. 3d and e). For metallacages **4b** and **4c**, downfield chemical shifts were observed for α-pyridyl protons H_a and β-pyridyl protons H_b compared with ligand **2** (Fig. 3f–h). Both H_a and H_b split into two sets of signals, which correspond to the protons inside and outside of the metallacages. In the 2D DOSY spectra, all the protons of metallacages **4b** and **4c** displayed a single diffusion coefficient (Fig. S13 and S17†), respectively, suggesting the formation of single discrete supramolecular structures. ESI-TOF-MS was carried out to afford the coordination stoichiometries of metallacages **4a–4c**. For metallacage **4a** (Fig. S7†), peaks at m/z = 1035.5970, 1180.2861, 1373.1576 and 1643.2198 were observed, corresponding to $[\mathbf{4a} + 8Na]^{8+}$, $[\mathbf{4a} + 7Na]^{7+}$, $[\mathbf{4a} + 6Na]^{6+}$ and $[\mathbf{4a} + 5Na]^{5+}$, respectively. For metallacages **4b** and **4c**, multiple prominent peaks of $[M–x(OTf)]^{x+}$ (x = 6–20) were observed, owing to the successive loss of counterions (OTf^-) (Fig. 3i and j). For instance, peaks at m/z = 1266.9769 and 1454.3884 were found, corresponding to $[\mathbf{4b}–9OTf]^{9+}$ and $[\mathbf{4c}–13OTf]^{13+}$, respectively. All the peaks were isotopically resolved and matched well with their theoretical distributions. These results are consistent with previous reports,[33–44] suggesting the successful formation of metallacages **4a–4c**.

Single crystals of metallacages **4a** and **4c** were obtained through the slow diffusion of dioxane into a DMF (for **4a**) or ethyl acetate into a DMSO (for **4c**) solution of the samples for more than two months. In the crystal structure of **4a**, four hexatopic carboxylic ligands were connected by 12 platinum(II) nodes, forming a truncated tetrahedron (Fig. 4a). The diameter of **4a** was 3.4 nm and the shortest Pt···Pt distance was 0.82 nm. The angle of O–Pt–O was *ca.* 84.1°, while the angle of P–Pt–P was *ca.* 97.8°. The size of **4a** is close to that of **4b** (Fig. 4b), whose

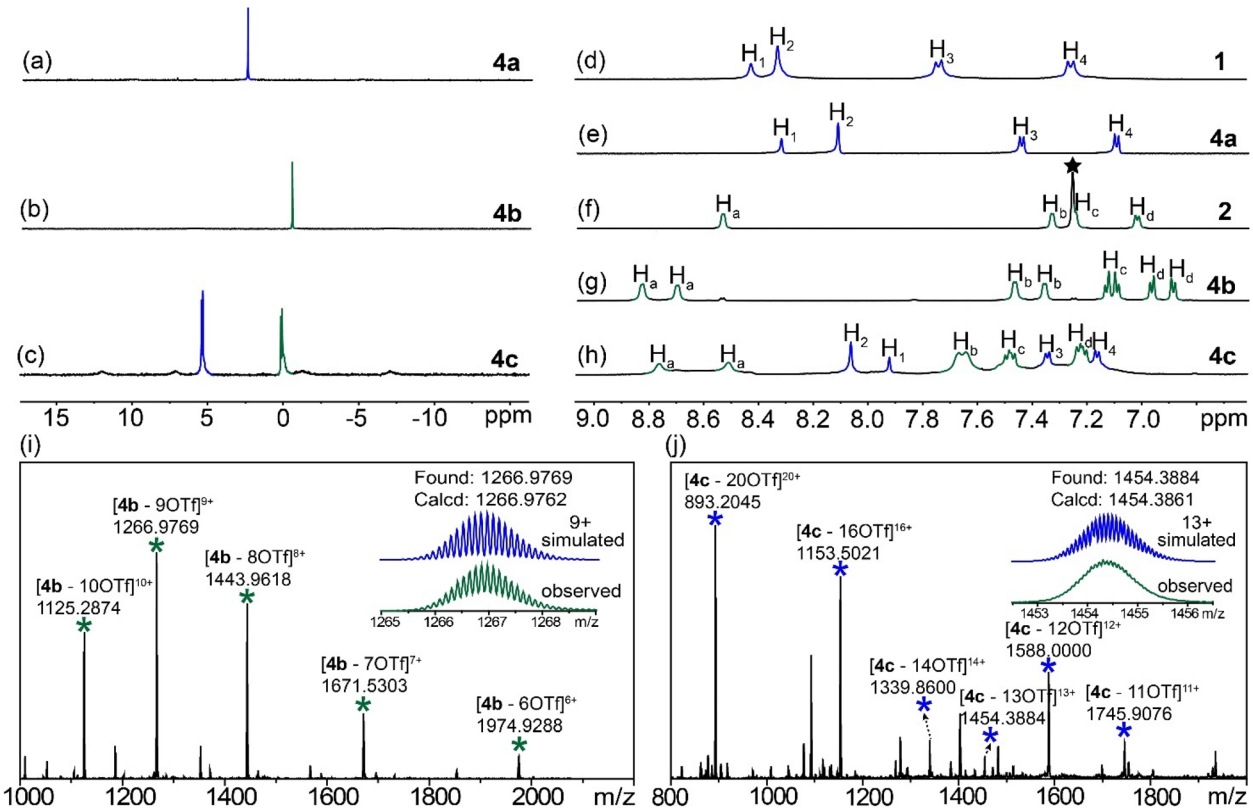

Fig. 3 Partial $^{31}P\{^1H\}$ NMR spectra (243 MHz, CD_3CN, 295 K) of (a) **4a**, (b) **4b** and (c) **4c**. Partial ^1H-NMR (600 MHz, 295 K) of (d) **1** (CD_3OD), (e) **4a** (CD_3CN), (f) **2** ($CDCl_3$), (g) **4b** (CD_3CN), and (h) **4c** (CD_3CN). The peak for $CHCl_3$ is marked with an asterisk. ESI-TOF-MS spectra of metallacages (i) **4b** and (j) **4c**.

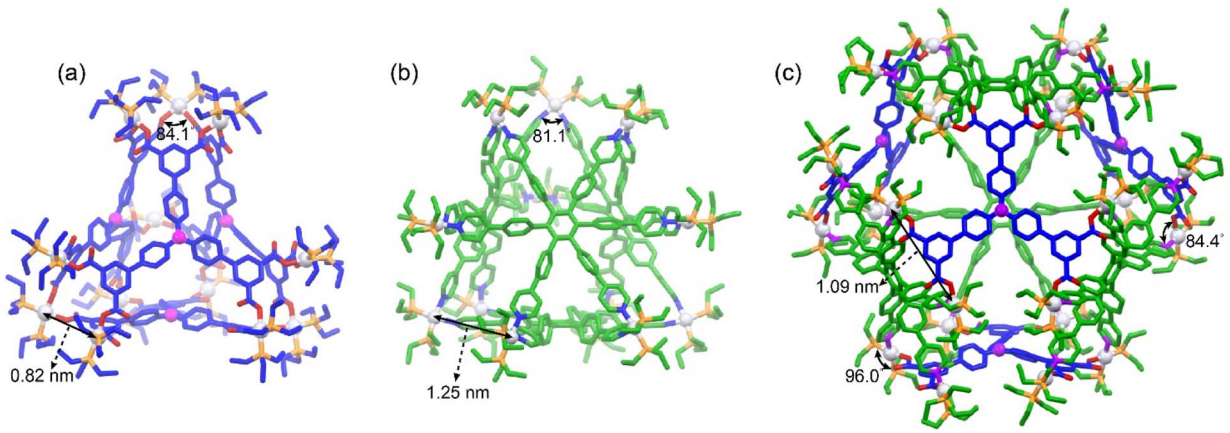

Fig. 4 (a)–(c) Crystal structures of metallacages **4a**, **4b** (ref. 45) and **4c**. Hydrogen atoms, counterions, and solvent molecules are omitted for clarity.

diameter reached 3.6 nm,[45] which would benefit their supramolecular fusion. For metallacage **4c**, four hexacarboxylic ligands (**1**) and four hexapyridyl units (**2**) were connected by 24 Pt nodes, forming a truncated octahedron with a diameter of 4.4 nm (Fig. 4c). Each carboxylic ligand was connected with its neighboring pyridyl unit through two O–Pt–N coordination bonds. The shortest Pt···Pt distance was 1.09 nm. The angle of O–Pt–N was *ca.* 84.4°, while the angle of P–Pt–P was *ca.* 96.0°. In the crystal packing of **4c** (Fig. S21†), regular packing was facilitated by non-covalent interactions between neighboring molecules, such as van der Waals force between the peripheral PEt_3 units and C–H···O hydrogen bonds. Due to the propeller-shaped structure of hexaphenylbenzene (HPB), the metallacages constructed with HPB as the main building block exhibit weak host–guest interactions with the common polycyclic aromatic hydrocarbon guest molecule (Fig. S30 and S31†).

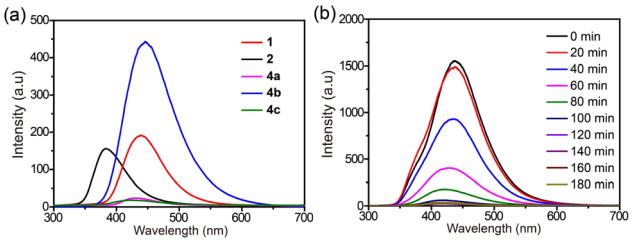

Fig. 5 (a) Fluorescence spectra of ligand **1** in CH_3CN/H_2O ($v : v = 9 : 1$), ligand **2** and metallacages **4a–4c** in CH_3CN. (b) Time-dependent fluorescence spectra of an equimolar mixture of **4a** and **4b** in CH_3CN. $\lambda_{ex} = 265$ nm and $c = 10.0$ μM.

To the best of our knowledge, metallacage **4a** represents the first neutral metallacage self-assembled from Pt nodes and multiple carboxylic ligands, while metallacage **4c** is the largest metallacage formed by the heteroleptic assembly of Pt nodes with both pyridyl and carboxylic ligands, which will promote the design and preparation of metallacages with advanced geometric structures.

UV/Vis absorption spectroscopy and fluorescence spectroscopy were conducted to investigate the photophysical properties of these ligands and metallacages. Ligands **1** and **2** displayed weak absorption bands centered at *ca.* 247 nm and 256 nm, with molar absorption coefficients (ε) of 3.67×10^4 and 1.50×10^4 M^{-1} cm^{-1}, respectively. Metallacages **4a** and **4b** exhibited dense absorption bands centered at *ca.* 354 nm and 276 nm, with ε of 9.27×10^4 and 1.83×10^5 M^{-1} cm^{-1}, respectively (Fig. S22†). Metallacage **4c** showed two absorption bands centered at *ca.* 297 and 342 nm (Fig. S22†), with ε of 3.07×10^5 and 1.09×10^5 M^{-1} cm^{-1}, respectively, which were derived from the absorption of ligands **1** and **2**. Metallacages **4a** and **4c** showed weak emission centered at *ca.* 433 and 420 nm, respectively, while bright emission centered at *ca.* 450 nm was observed for metallacage **4b** (Fig. 5a). The weak emission of **4a** and **4c** was due to the photoinduced electron transfer,[47] while the bright emission of **4b** was because of the restriction of molecular motions by metal-coordination bonds,[48,49] which has also been observed in other supramolecular systems.[50,51]

The distinct fluorescence characteristics of these metallacages provide a visual method to monitor their assembly and fusion processes by using the changes in fluorescence as output signals. Mixing **4a** and **4b** in a 1 : 1 molar ratio resulted in a gradually decreased emission over time, accompanied by

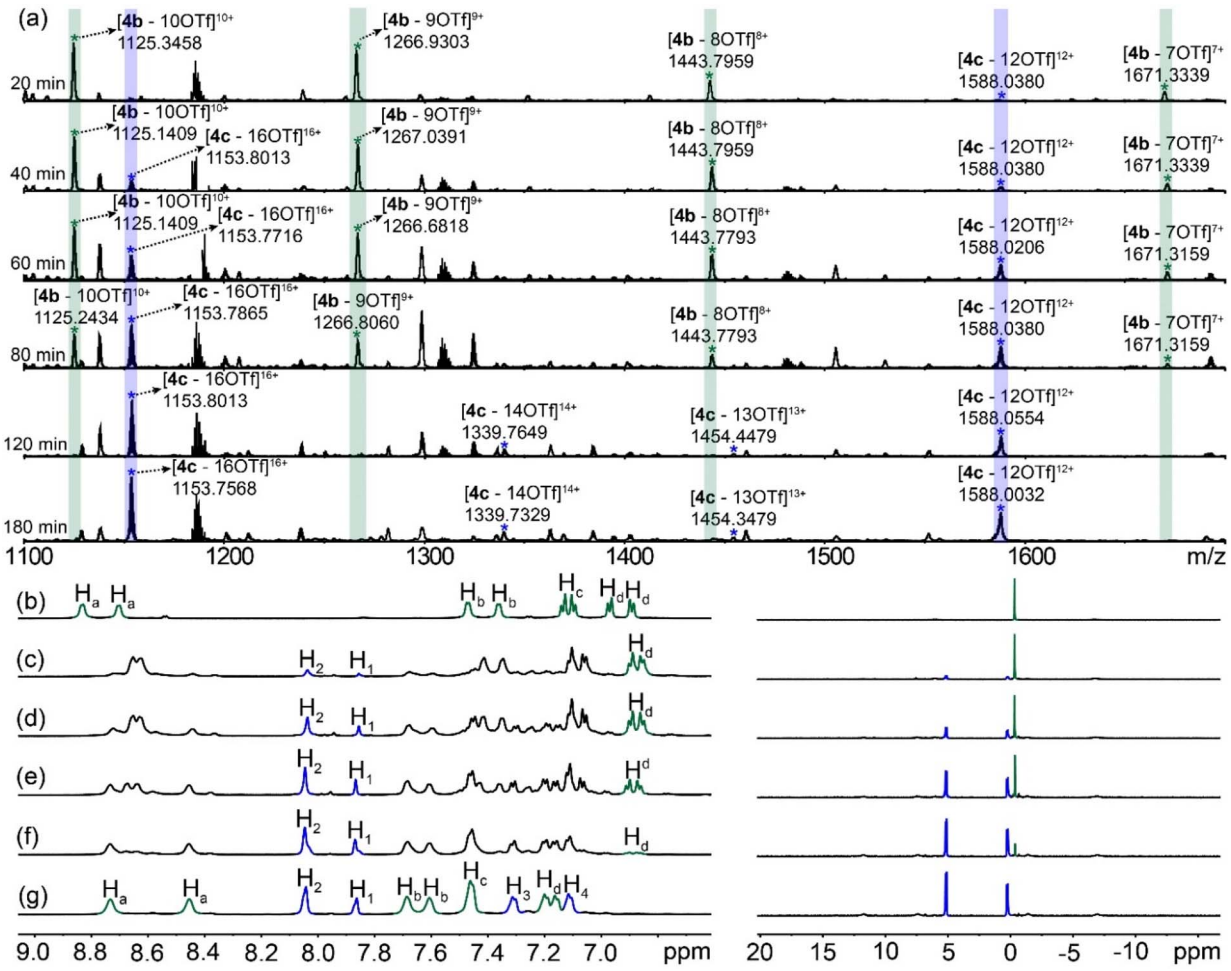

Fig. 6 (a) Time-dependent ESI-TOF-MS spectra of the mixture of **4a** and **4b** ($c = 500.0$ μM). Partial ^1H (600 MHz) and $^{31}P\{^1H\}$ NMR (243 MHz) spectra of (b) **4b**, and **4b** with (c) 0.2, (d) 0.4, (e) 0.6, (f) 0.8 and (g) 1.0 equivalents of **4a** (CD_3CN at 295 K).

a blueshift of the maximum emission (Fig. 5b). After 120 min, negligible changes were observed from the fluorescence spectra (Fig. S23†), suggesting that the reaction reached an equilibrium state and that the supramolecular fusion of geometrically similar **4a** and **4b** into **4c** was complete in 120 min.

ESI-TOF-MS was also carried out to study the kinetics of the fusion (Fig. 6a). Acetonitrile solutions containing the same amount of **4a** and **4b** were stirred at 60 °C and the ESI-TOF-MS spectra were collected at different time points. After 20 min, the peaks corresponding to **4c** started to appear, suggesting that the fusion process began to take place at this time point. As time progressed, the signals of **4b** gradually decreased, while those of **4c** increased. After 120 min, only the signals of **4c** were observed from the spectra, which agreed well with the fluorescence data, indicating that the fusion of **4a** and **4b** was complete.

The concentration-dependent fusion between **4a** and **4b** was investigated by NMR spectroscopy. The gradual addition of **4a** into the acetonitrile solution of **4b** resulted in significant changes in the NMR spectra (Fig. 6b–g). The peaks of protons H_a shifted upfield. while downfield chemical shifts were found for protons H_b, H_c and H_d. Two new peaks, derived from protons H_1 and H_2 of **4a**, gradually emerged. After the addition of 1.0 equivalent of **4a** into **4b**, the ^{1}H NMR spectrum matched well with that of **4c**, suggesting a quantitative transformation from the mixture of **4a** and **4b** to **4c**. In the $^{31}P\{^1H\}$ NMR spectra, the single peak of **4b** slowly disappeared, while two doublet peaks corresponding to **4c** were observed over time. Moreover, the variations in solvent and counterions showed little influence on the formation of **4c** (Fig. S26–29†). Therefore, the fusion process of these assemblies was fully tracked and supported by the combination of fluorescence, mass and NMR spectroscopy, which provides a good example for the construction of supramolecular assemblies with improved structural complexity *via* supramolecular fusion. To understand the mechanism of the fusion from two truncated tetrahedron-shaped metallacages, we compared the energies of the sum of the two homoleptic $M_{12}L_4$ metallacages with that of **4c** using the semiempirical GFN1-xTB method. According to the comparison between the energy values of metallacages, the energy of **4c** is significantly lower than the sum of the energies of the homoleptic metallacages (Fig. S32†), suggesting that the assembly of **4c** is enthalpically more favorable.

Conclusions

In summary, a neutral truncated tetrahedron and a giant truncated octahedron were successfully prepared by metal-coordination-driven self-assembly. Interestingly, the neutral truncated tetrahedron could be quantitatively transformed into the truncated octahedron *via* its further assembly with another cationic truncated tetrahedron, representing a supramolecular fusion at the three-dimensional level from geometrically the same truncated tetrahedron-shaped metallacages. The fundamental knowledge obtained from the current research not only shows the process of supramolecular fusion, but also provides a simple and efficient strategy for preparing supramolecular assemblies with enhanced structural complexity and integrated functions.

Data availability

The data supporting this article have been included in the ESI.† Crystallographic data for **4a** (2314346) and **4c** (2314347) have been deposited at the Cambridge Crystallographic Data Centre.

Author contributions

M. Zhang and H. Liu conceived the project. H. Liu and Y. Huang carried out the synthesis and some characterization experiments of the compounds. C. Guo carried out the ESI-TOF-MS tests and analyzed the data. Z. Zhou, S. Jian, Z. Zhang, and Y. Hou assisted in the synthesis and characterization of the compounds. The manuscript was written by H. Liu, C. Mu, and M. Zhang and all authors contributed to the final draft of the paper.

Conflicts of interest

The authors declare no competing financial interests.

Acknowledgements

This work was supported by the National Natural Science Foundation of China (22171219 and 22222112), the Innovation Talent Promotion Plan of Shaanxi Province for Science and Technology Innovation Team (2023-CX-TD-51), and the Fundamental Research Funds for the Central Universities. We thank Dr Gang Chang and Dan He at the Instrument Analysis Center of Xi'an Jiaotong University for the NMR and fluorescence measurements. We also thank Dr Zhenyi Zhang from Bruker (Beijing) Scientific Technology in Shanghai for the X-ray crystal structure analysis.

References

1 Y. Yuan, M. F. Tam, V. Simplaceanu and C. Ho, *Chem. Rev.*, 2015, **115**, 1702–1724.
2 G. P. Lisi and J. P. Loria, *Chem. Rev.*, 2016, **116**, 6323–6636.
3 K. W. Chen, T. Y. Sun and Y. D. Wu, *Chem. Rev.*, 2023, **123**, 9940–9981.
4 J. J. Vittal, *Coord. Chem. Rev.*, 2007, **251**, 1781–1795.
5 W. Wang, Y. X. Wang and H. B. Yang, *Chem. Soc. Rev.*, 2016, **45**, 2656–2693.
6 Y. Gong, Y. Zhang, C. Qin, C. Sun, X. Wang and Z. Su, *Angew. Chem., Int. Ed.*, 2019, **58**, 780–784.
7 D. Zhang, Q. Gan, A. J. Plajer, R. Lavendomme, T. K. Ronson, Z. Lu, J. D. Jensen, B. W. Laursen and J. R. Nitschke, *J. Am. Chem. Soc.*, 2022, **144**, 1106–1112.
8 A. Walther, I. Regeni, J. J. Holstein and G. H. Clever, *J. Am. Chem. Soc.*, 2023, **145**, 25365–25371.
9 G. Li, Z. Zhou, C. Yuan, Z. Guo, Y. Liu, D. Zhao, K. Liu, J. Zhao, H. Tan and X. Yan, *Angew. Chem., Int. Ed.*, 2020, **59**, 10013–10017.
10 C. F. Espinosa, T. K. Ronson and J. R. Nitschke, *J. Am. Chem. Soc.*, 2023, **145**, 9965–9969.

11 E. Zangrando, M. Casanova and E. Alessio, *Chem. Rev.*, 2008, **108**, 4979–5013.
12 T. R. Cook and P. J. Stang, *Chem. Rev.*, 2015, **115**, 7001–7045.
13 T. R. Cook, V. Vajpayee, M. H. Lee, P. J. Stang and K. W. Chi, *Acc. Chem. Res.*, 2019, **46**, 2464–2474.
14 M. Yoshizawa, M. Tamura and M. Fujita, *Science*, 2006, **312**, 251–254.
15 M. D. Wise, J. J. Holstein, P. Pattison, C. Besnard, E. Solari, R. Scopelliti, G. Bricogne and K. Severin, *Chem. Sci.*, 2015, **6**, 1004–1010.
16 T. Tsutsui, L. Catti, K. Yoza and M. Yoshizawa, *Chem. Sci.*, 2020, **11**, 8145–8150.
17 T. Z. Xie, K. J. Endres, Z. Guo, J. M. Ludlow III, C. N. Moorefield, M. J. Saunders, C. Wesdemiotis and G. R. Newkome, *J. Am. Chem. Soc.*, 2016, **138**, 12344–12347.
18 J. E. M. Lewis, E. L. Gavey, S. A. Cameron and J. D. Crowley, *Chem. Sci.*, 2012, **3**, 778–784.
19 R. L. Spicer, A. D. Stergiou, T. A. Young, F. Duarte, M. D. Symes and P. J. Lusby, *J. Am. Chem. Soc.*, 2020, **142**, 2134–2139.
20 P. Howlader, S. Mondal, S. Ahmed and P. S. Mukherjee, *J. Am. Chem. Soc.*, 2020, **142**, 20968–20972.
21 D. N. Yan, L. X. Cai, P. M. Cheng, S. J. Hu, L. P. Zhou and Q. F. Sun, *J. Am. Chem. Soc.*, 2021, **143**, 16087–16094.
22 R.-J. Li, A. Marcus, F. Fadaei-Tirani and K. Severin, *Chem. Commun.*, 2021, **57**, 10023–10026.
23 Y. Li, J. Dong, W. Gong, X. Tang, Y. Liu, Y. Cui and Y. Liu, *J. Am. Chem. Soc.*, 2021, **143**, 20939–20951.
24 A. Kumar, S. S. Sun and A. J. Lees, *Coord. Chem. Rev.*, 2008, **252**, 922–939.
25 M. D. Ward, C. A. Hunter and N. H. Williams, *Acc. Chem. Res.*, 2018, **51**, 2073–2082.
26 K. Niki, T. Tsutsui, M. Yamashina, M. Akita and M. Yoshizawa, *Angew. Chem., Int. Ed.*, 2020, **59**, 10489–10492.
27 Y. Tamura, H. Takezawa and M. Fujita, *J. Am. Chem. Soc.*, 2020, **142**, 5504–5508.
28 P. Mal, B. Breiner, K. Rissanen and J. R. Nitschke, *Science*, 2009, **324**, 1697–1699.
29 G. R. Genov, H. Takezawa, H. Hayakawa and M. Fujita, *J. Am. Chem. Soc.*, 2023, **145**, 17013–17017.
30 Y. R. Zheng, Z. Zhao, M. Wang, K. Ghosh, J. B. Pollock, T. R. Cook and P. J. Stang, *J. Am. Chem. Soc.*, 2010, **132**, 16873–16882.
31 A. K. Bar, G. Mostafa and P. S. Mukherjee, *Inorg. Chem.*, 2010, **49**, 7647–7649.
32 A. K. Bar, S. Raghothama, D. Moon and P. S. Mukherjee, *Chem.–Eur. J.*, 2012, **18**, 3199–3209.
33 Y. Hou, Z. Zhang, S. Lu, J. Yuan, Q. Zhu, W. P. Chen, S. Ling, X. Li, Y. Z. Zheng, K. Zhu and M. Zhang, *J. Am. Chem. Soc.*, 2020, **142**, 18763–18768.
34 C. Mu, Z. Zhang, Y. Hou, H. Liu, L. Ma, X. Li, S. Ling, G. He and M. Zhang, *Angew. Chem., Int. Ed.*, 2021, **60**, 12293–12297.
35 Y. Hou, R. Shi, H. Yuan and M. Zhang, *Chin. Chem. Lett.*, 2023, **34**, 107688.
36 Z. Zhang, L. Ma, F. Fang, Y. Hou, C. Lu, C. Mu, Y. Zhang, H. Liu, K. Gao, M. Wang, Z. Zhang, X. Li and M. Zhang, *JACS Au*, 2022, **2**, 1479–1487.
37 Q. Feng, T. Yang, L. Ma, X. Li, H. Yuan, M. Zhang, Y. Zhang and L. Fan, *ACS Appl. Mater. Interfaces*, 2022, **14**, 38594–38603.
38 Y. Hou, Z. Zhang, L. Ma, R. Shi, S. Ling, X. Li and M. Zhang, *CCS Chem.*, 2022, **4**, 2604–2611.
39 H. Liu, Z. Zhang, C. Mu, L. Ma, H. Yuan, S. Ling, H. Wang, X. Li and M. Zhang, *Angew. Chem., Int. Ed.*, 2022, **61**, e202207289.
40 Q. Feng, N. Li, Z. Zhang, K. Gao, K. Wang, S. Ling, H. Yuan, Y. Zhang and M. Zhang, *Chin. Chem. Lett.*, 2023, **34**, 108439.
41 H. Liu, C. Guo, Z. Zhang, C. Mu, Q. Feng and M. Zhang, *Chem.–Eur. J.*, 2023, **29**, e202203926.
42 H. Duan, T. Yang, Q. Li, F. Cao, P. Wang and L. Cao, *Chin. Chem. Lett.*, 2024, **3**, 108878.
43 R. Zhang, D. Hu, Y. Fu, Q. Feng, C. Mu, K. Gao, H. Ma, M. Liu and M. Zhang, *Aggregate*, 2024, **5**, e408.
44 Y. Hou, C. Mu, Y. Shi, Z. Zhang, H. Liu, Z. Zhou, S. Ling, B. Shi, X. Duan, C. Yang and M. Zhang, *Aggregate*, 2024, e628.
45 Y. R. Zheng, Z. Zhao, H. Kim, M. Wang, K. Ghosh, J. B. Pollock, K. W. Chi and P. J. Stang, *Inorg. Chem.*, 2010, **49**, 10238–10240.
46 Z. Guo, G. Li, H. Wang, J. Zhao, Y. Liu, H. Tan, X. Li, P. J. Stang and X. Yan, *J. Am. Chem. Soc.*, 2021, **143**, 9215–9221.
47 J. L. Zhu, L. Xu, Y. Y. Ren, Y. Zhang, X. Liu, G. Q. Yin, B. Sun, X. Cao, Z. Chen, X. L. Zhao, H. Tan, J. Chen, X. Li and H. B. Yang, *Nat. Commun.*, 2019, **10**, 4285.
48 J. Mei, N. L. Leung, R. T. Kwok, J. W. Y. Lam and B. Z. Tang, *Chem. Rev.*, 2015, **115**, 11718–11940.
49 Z. Zhao, H. Zhang, J. W. Y. Lam and B. Z. Tang, *Angew. Chem., Int. Ed.*, 2020, **59**, 9888–9907.
50 L. J. Chen, Y. Y. Ren, N. W. Wu, B. Sun, J. Q. Ma, L. Zhang, H. Tan, M. Liu, X. Li and H. B. Yang, *J. Am. Chem. Soc.*, 2015, **137**, 11725–11735.
51 P. Das, A. Kumar, P. Howlader and P. S. Mukherjee, *Chem.–Eur. J.*, 2017, **23**, 12565–12574.